Neuroscience 158 (2009) 1509–1520

AGE-RELATED REDUCTION IN MICROCOLUMNAR STRUCTURE CORRELATES WITH COGNITIVE DECLINE IN VENTRAL BUT NOT DORSAL AREA 46 OF THE RHESUS MONKEY

L. CRUZ,[a]* D. L. ROE,[c] B. URBANC,[a] A. INGLIS,[b] H. E. STANLEY[b] AND D. L. ROSENE[c,d]

[a]*Department of Physics, 3141 Chestnut Street, Drexel University, Philadelphia, PA 19104, USA*

[b]*Center for Polymer Studies and Department of Physics, Boston University, Boston, MA 02215, USA*

[c]*Department of Anatomy and Neurobiology, Boston University School of Medicine, Boston, MA 02118, USA*

[d]*Yerkes National Primate Research Center, Emory University, Atlanta, GA 30322, USA*

Abstract—The age-related decline in cognitive function that is observed in normal aging monkeys and humans occurs without significant loss of cortical neurons. This suggests that cognitive impairment results from subtle, sub-lethal changes in the cortex. Recently, changes in the structural coherence in mini- or microcolumns without loss of neurons have been linked to loss of function. Here we use a density map method to quantify microcolumnar structure in both banks of the sulcus principalis (prefrontal cortical area 46) of 16 (ventral) and 19 (dorsal) behaviorally tested female rhesus monkeys from 6 to 33 years of age. While total neuronal density does not change with age in either of these banks, there is a significant age-related reduction in the strength of microcolumns in both regions on the order of 40%. This likely reflects a subtle but definite loss of organization in the structure of the cortical microcolumn. The reduction in strength in ventral area 46 correlates with cognitive impairments in learning and memory while the reduction in dorsal area 46 does not. This result is congruent with published data attributing cognitive functions to ventral area 46 that are similar to our particular cognitive battery which does not optimally tap cognitive functions attributed to dorsal area 46. While the exact mechanisms underlying this loss of microcolumnar organization remain to be determined, it is plausible that they reflect age-related alterations in dendritic and/or axonal organization which alter connectivity and may contribute to age-related declines in cognitive performance.

Key words: aging, cognition, minicolumns, microcolumns, neuronal organization, primate brain.

While conventional wisdom posits that age-related cognitive decline is the result of age-related neuronal loss, this notion has not stood up to experimental scrutiny. Recent studies have asserted that cognitive decline in normal aging, in contrast to other age-related neurodegenerative disorders such as Alzheimer's disease, is not accompanied by significant loss of neurons in the cerebral cortex (e.g. Pakkenberg and Gundersen, 1997; Peters et al., 1998; Pakkenberg et al., 2003). Considerable evidence has instead implicated other brain changes including changes in synapses, dendrites, and white matter that would likely alter cortical information processing and may therefore better account for age-related cognitive decline (e.g. Peters and Rosene, 2003). This evidence does not rule out other subtle changes that might be occurring in gray matter and that may equally well contribute to cortical dysfunction. One important feature of the cortex, and a possibly vulnerable element, is the vertical arrays of neurons called minicolumns. Minicolumns, or "microcolumns" as referred to in this paper, are usually found spanning from the subcortical white matter to the pial surface (Mountcastle, 1997, 2003). Microcolumns sometimes share terminology with other possibly related intracortical elements such as bundles of apical dendrites (Peters, 1994; Rockland and Ichinohe, 2004) or axons of pyramidal cells and pyramidal cell modules (DeFelipe et al., 1990; Jones, 2000). Following the early physiological studies by Mountcastle (1957) and Hubel and Wiesel (1963, 1969, 1977) on the much larger macrocolumns, microcolumns have been characterized as a fundamental unit of organization and function (Mountcastle, 1997, 2003; Peters and Sethares, 1996; Constantinidis et al., 2001; Buxhoeveden and Casanova, 2002; Vercelli et al., 2004). This characterization, however, is not universally accepted as numerous critiques question the validity of the microcolumn as a fundamental unit of organization or function (Swindale, 1990; Purves et al., 1992; Jones, 2000; Rockland and Ichinohe, 2004; Buxhoeveden and Casanova, 2005; Krieger et al., 2007). Other studies of "whisker columns" or barrels in the rodent somatosensory cortex (the anatomical equivalent of a functional cortical column) indicate that these columns are not a functional unit consisting of cells with similar functional properties (Helmstaedter et al., 2007). Even further, others argue that the very well established and much studied ocular dominance columns seem not to serve a purpose (Horton and Adams, 2005).

Independent of the exact function of the microcolumn, a growing body of studies has reported structural changes in microcolumns that are related to a general loss of cognitive function in normal aging and in various disease states. These studies have dealt with differences in neuron distribution in general, and within microcolumns in particular, and span topics from normal aging (Cruz et al., 2004),

*Corresponding author. Tel: +1-215-895-1989; fax: +1-215-895-5934.
E-mail address: ccruz@drexel.edu (L. Cruz).

Abbreviations: CII, Cognitive Impairment Index; DNMS, Delayed Non-match to Sample; DNMS-10, Delayed Non-match to Sample test at a 10 s delay; DNMS-120, Delayed Non-match to Sample test at a 2 min delay; DRST, Delayed Recognition Span Task; ROI, region of interest; 46D, dorsal 46; 46V, ventral 46.

0306-4522/09 © 2009 IBRO. Published by Elsevier Ltd. All rights reserved.
doi:10.1016/j.neuroscience.2008.11.033

Alzheimer's disease and Lewy body dementia (Van Hoesen and Solodkin, 1993; Buldyrev et al., 2000), schizophrenia (Benes and Bird, 1987; Buxhoeveden et al., 2000), Down syndrome (Buxhoeveden et al., 2002), autism (Casanova et al., 2003), dyslexia (Casanova et al., 2002), to drug (cocaine) manipulation during development (Buxhoeveden et al., 2006). Interestingly, while we have noted that the number of cortical neurons is largely preserved in normal aging monkeys, evidence of age-related physiological disruption of orientation selective microcolumns has been reported (Schmolesky et al., 2000; Leventhal et al., 2003). These investigators reported a loss of orientation and direction selectivity in microcolumns in V1 and demonstrated that administration of GABA agonists temporarily restored normal stimulus selectivity to these neurons. Since small GABAergic interneurons are an important, though poorly understood, component of the microcolumn (Mountcastle, 1997) this suggests that there may well be a disruption within the microcolumn as part of normal aging.

We previously reported a 40% loss of microcolumnar strength in area 46 of the ventral bank of sulcus principalis in aging monkeys and determined that this loss of strength correlates with cognitive decline (Cruz et al., 2004). In the present study, we examine age-related changes in microcolumns in tissue from a larger cohort of normal aging monkeys and compare microcolumnarity in area 46 of the prefrontal cortex in the upper (dorsal) and lower (ventral) banks of the mid level of sulcus principalis. In terms of function, damage to the lateral prefrontal cortex, including areas 9, 46, and 9/46, is well-known to cause deficits in performance of tasks requiring executive functions, noting that this broad area also takes part in operations that include abstraction, response selection, working memory operations, memory encoding and retrieval. Data from humans and monkeys, as reviewed by Petrides (2005), suggest that for the midlateral prefrontal cortices that we examine, ventral area 46 is likely involved in processing information in conjunction with the posterior parietal, temporal, and occipital association cortices for both the encoding and retrieval aspects of memory processes. In contrast, dorsal area 46 is likely involved in monitoring working memory operations important for processes such as abstraction or set shifting.

To quantify the microcolumnar structure of these two areas we apply a density map analysis (Cruz et al., 2005) to images from ventral 46 (46V) and dorsal 46 (46D) from a cohort of 19 normal aging female rhesus monkeys. The goal of this comparison is to determine if the previously observed loss of microcolumnar strength reported in a smaller cohort for 46V (Cruz et al., 2004) is localized to 46V or a more global age-related effect, and to explore the possibility that changes in these areas are related to their specific cognitive functions.

EXPERIMENTAL PROCEDURES

Subjects

Brain tissue was obtained from 19 female rhesus monkeys ranging from 6.4–32.9 years of age. This material was derived from archived tissue samples available from a study of the neural bases of age-related cognitive decline. Hence no animals were utilized explicitly for this study. Under the procedures of that study, animals were selected from the population of monkeys at the Yerkes National Primate Research Center (YNPRC) at Emory University according to strict selection criteria that excluded any monkeys with health or experimental histories that could have affected the brain or cognitive function. The lifespan of the rhesus monkey compared with the human corresponds approximately to a ratio of 1:3 (Tigges et al., 1988). Monkeys therefore can be considered young adults at age 5 when they reach sexual maturity, which would roughly correspond to a 15-year-old human. Few monkeys live beyond 30 years of age, which would roughly correspond to humans over 90 years old (Tigges et al., 1988; Roth et al., 2004).

Animal procedures

After entering the study monkeys were first maintained at the YNPRC, and subsequently at the Laboratory Animal Science Center of the Boston University Medical Center. Both facilities are fully accredited by the Association for the Assessment and Accreditation of Laboratory Animal Care. All procedures were approved by the Institutional Animal Care and Use Committee of both Emory University and Boston University Medical Campus, and conformed to the NIH *Guide for the Care and Use of Laboratory Animals* and the U.S. *Public Health Service Policy on Humane Care and Use of Laboratory Animals*. Monkeys received initial Magnetic Resonance Imaging (MRI) scans (Intera 3T Scanner, Phillips Instruments, North Andover, MA, USA) to ensure there was no occult pathology in the brain and then were tested on a battery of cognitive tests to characterize learning and memory (e.g. Herndon et al., 1997) and executive function (Moore et al., 2005). At the conclusion, monkeys were tranquilized with ketamine hydrochloride, deeply anesthetized with sodium pentobarbital, and killed by exsanguination during transcardial perfusion of the brain with 4–8 l of warm (37 °C) fixative containing either 4% paraformaldehyde alone or a mixture of 1% paraformaldehyde and 1.25% glutaraldehyde in 0.1 M phosphate buffer (pH 7.4). Immediately after perfusion fixation of the brain, the brain was blocked, *in situ*, in the coronal stereotactic plane. One hemisphere was then cryoprotected in graded solutions culminating with 20% glycerol and 2% DMSO in phosphate buffer (0.1 M, pH 7.4) after which the blocks were flash frozen by immersion in −75 °C isopentane (Rosene et al., 1986). All blocks were stored at −80 °C until cut.

Tissue processing

Frozen blocks were oriented on the freezing stage of a sledge microtome and frozen sections cut in the coronal stereotactic plane into eight interrupted series of 30 μm thick sections and one series of 60 μm thick sections so that sections in each series were spaced 300 μm apart. One 30 μm thick series and the 60 μm thick series were mounted on subbed microscope slides, allowed to dry overnight and then stained for Nissl substance with Thionin, dehydrated, cleared, and coverslipped. This cryoprotection and cutting procedure produced minimal shrinkage or distortion so that (x,y,z) dimensions were largely preserved through the cutting procedure (Rosene et al., 1986). Once mounted, the sections adhered rapidly to the subbed surface of the slide before they dried, preserving the x–y relationships within the section which was a requisite for all of our analyses described below. However, as sections dried and were subsequently stained, dehydrated and coverslipped, they shrank in the z dimension (thickness) from the originally cut thickness of 30 μm to an average mounted section thickness of 7–10 μm, as determined using the Bioquant Image Analysis system (Bioquant Inc, Nashville, TN, USA) equipped with a Heidenhain stage micrometer that measured z axis position to 0.1 μm. Hence the analysis of neuronal locations was limited to this collapsed x-y projection as discussed below.

Cytoarchitectonic regions to be studied

Area 46 is a neocortical subdivision of the prefrontal cortex that is implicated in working memory and executive functions (Goldman and Rosvold, 1970; Goldman et al., 1971; Goldman-Rakic, 1988; Petrides, 2000a,b; Moore et al., 2002a,b). Area 46 in the upper and lower bank of the middle part of sulcus principalis was selected for study, where in coronal sections the cortex is relatively flat (Fig. 1a and b). Our analysis was limited to layer 3 of area 46 for several reasons. First, layer 3 is where the majority of cortico-cortical projections that subserve cortical information transfer originate and where the cortico-cortical projecting pyramidal cells have been most carefully studied (e.g. Page et al., 2002; Duan et al., 2003; Chang et al., 2005) making this layer particularly pertinent to the cortical cognitive functions that change with age. Second, as shown in Fig. 1c and d, neurons in layer 3 are relatively loosely packed compared with the smaller, more tightly packed neurons found in adjacent layers 2 and 4. This fact facilitated the reliable identification of neurons, a requirement for our quantitative analysis. Third, because microcolumns span from layer 6 to layer 2 and spacing and other features vary widely across layers, a composite average from all layers would obscure real features. Since analysis of all of the layers of cortex was beyond the scope of our technical capacity, we chose to limit this investigation to layer 3 for the reasons cited as well as to follow up on our previous investigation (Cruz et al., 2004). Due to this restriction, however, we cannot yet assess whether columnarity in other layers is affected by age, or how they may relate to cognitive functions.

Digital photography

Two 30 μm thick Nissl-stained sections per case spaced 300–600 μm apart from area 46 in the middle third of the sulcus principalis were selected (Fig. 1a and b) according to the architectonic criteria of Petrides and Pandya (1994). The levels were matched across all cases. A series of photomicrographs from both banks of sulcus principalis was digitized from both sections with a

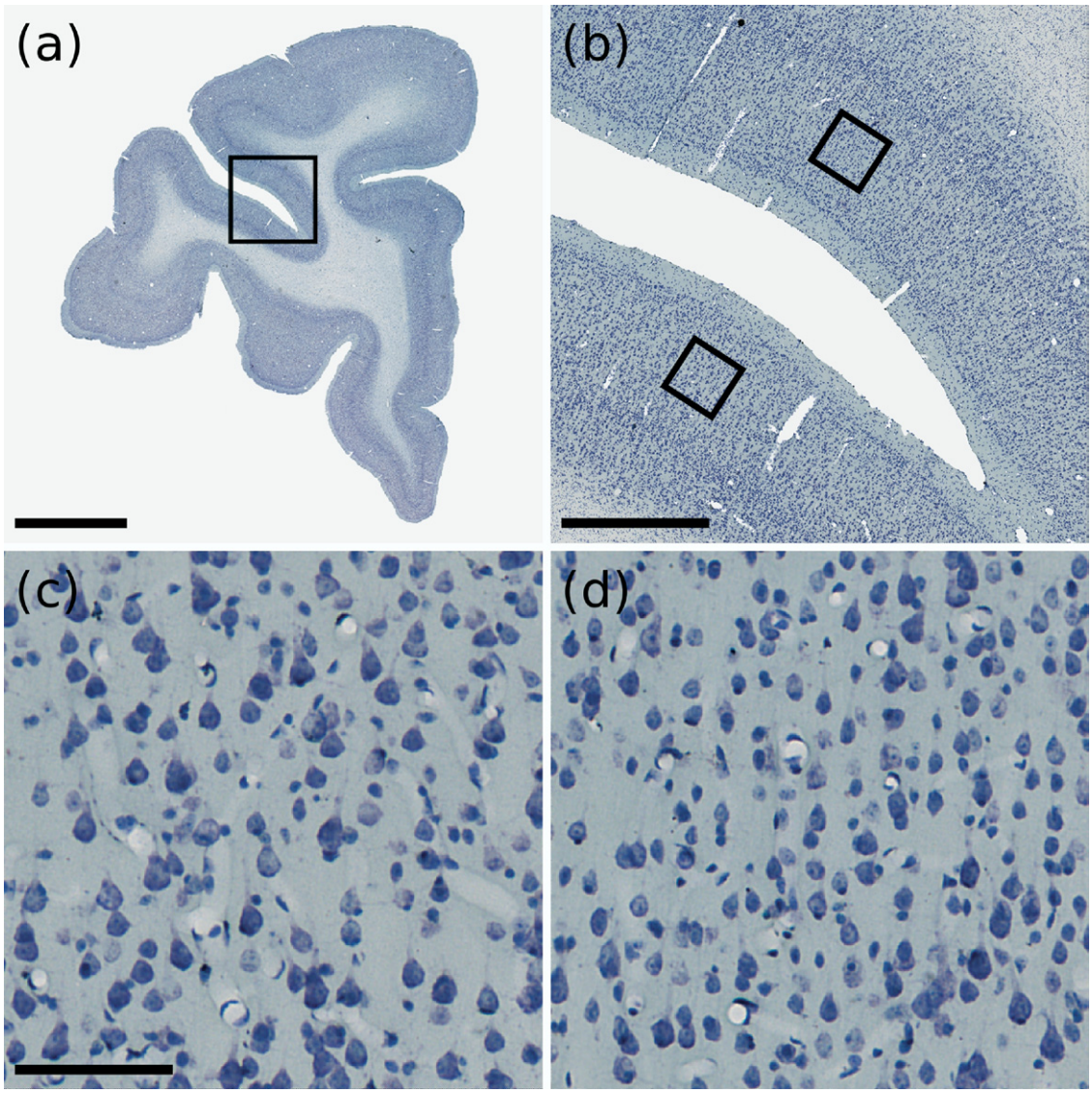

Fig. 1. (a) A coronal section of the frontal lobe at the level of the sulcus principalis, area 46, where photographs were digitized (scale=5 mm). (b) A higher magnification of the boxed area from (a) with two boxes delineating areas of layer 3 from the ventral (bottom) and dorsal (top) banks of the sulcus illustrating the location of layer 3 (scale=1 mm). (c, d) Higher magnification photomicrographs of the boxes in (b) illustrating typical images that were analyzed using the density map method. (c) Ventral and (d) dorsal bank of the sulcus principalis (scale bar=100 μm for both panels).

digital camera at 1280×1024 resolution using a 10× objective on a Nikon E600 microscope (Nikon Inc, Melville, NY, USA). These photomicrographs spanned from the bottom of layer 1 through the top of layer 4 and were then cropped such that a square central area of resolution 512×512 pixels was entirely inside layer 3 (Fig. 1c and d). In each bank of the sulcus, four adjacent (non-overlapping) 10× images of layer 3 were acquired. Due to differences in acquisition equipment used, there were slight differences in digital magnification across subjects, where all images for each subject had areas of either 320 μm×320 μm (1.6 pixels per μm), 332 μm×332 μm (1.54 pixels per μm), or 341 μm×341 μm (1.5 pixels per μm). Images from dorsal area 46 from all 19 monkeys were acquired, but due to tissue artifacts images from ventral area 46 in only 16 of the 19 monkeys were acquired. Also, small regions in the images containing tissue folds, large blood vessels, or other artifacts were computationally excluded to avoid including areas of the tissue from which no neuronal data were obtained. In total, eight images (four photomicrographs×two sections of area 46) from each of 19 subjects in dorsal area 46 and from 16 of those subjects in ventral area 46 were analyzed for a total of 280 images.

Identification of *x,y* coordinates of neurons

To locate all of the neurons in every image, a semi-automatic method of neuron detection was first applied (Cruz et al., 2005) to get the majority of the neuronal locations with an accuracy of about 80–85% but with the disadvantage of obtaining about 15–20% false positives. Using an off-the-shelf image editing program, all of these neuronal markings were then manually corrected to eliminate the false positives and to add the missed neurons in every image after which the final (x,y) coordinates for detected neurons were recorded. All of these (x,y) coordinates were independently corroborated using our newly developed automated neuron recognition algorithm (ANRA) (Inglis et al., 2008) optimized for layer 3 of the cortex.

Density map method and microcolumnar quantities

Microcolumns are vertical arrays of neurons with dimensions in the micrometer scale (Jones, 2000). Fig. 2 shows an example of neurons that line up in a fashion typical of layer 3 microcolumns. To characterize the degree of microcolumnarity of a region of tissue, we developed the density map method that can be used to quantitatively assess and compare different regions in terms of degree of microcolumnarity. This density map method was initially presented by Buldyrev et al. (2000) and a more detailed quantification and validation was given in Cruz et al. (2005). Briefly, the density map method calculates the density correlation function $g(x,y)$ using as input the (x,y) neuronal coordinates from an image. This function $g(x,y)$ can be mapped to a two-dimensional gray-scale image in which different shades of gray are proportional to the average neuronal density relative to the location of each neuron in the region of interest (ROI). This quantity represents the local neuronal density at a particular location (x,y) as opposed to the global neuronal density that specifies the sample-wide average neuronal density with a single number. Thus, the density map represents the average neuronal neighborhood (local) surrounding a typical neuron within a larger ROI.

Operationally, the density map is calculated by first assigning indices ($i=1,2,3 \ldots N$) to all the neurons in the sample. Next, we define an origin outside of the sample (Fig. 3a) and create a copy of the locations for the neuron labeled *1* and shift this copy so that neuron *1* overlays the origin (Fig. 3b). This process is repeated for each of the detected neurons (Fig. 3c) until an overlay of N copies of the locations in the sample is obtained (Fig. 3d, right image). Over this overlay we then center a grid of bins of size D (Fig. 3d) and count how many neurons fall in each bin, thus constructing one matrix (from the grid) of accumulated neurons $m(x,y)$ for the sample. We define $g(x,y)=m(x,y)/ND^2$, in which $g(x,y)$ has units of an average density of objects at position (x,y). This density function would be uniform if locations of objects (neurons) are uncorrelated, but will show patterns when there are any spatial correlations between the objects. For the case of neurons forming microcolumns in the cortex, their density map exhibits one central vertical ridge, sometimes accompanied by two less pronounced parallel neighboring ridges (Fig. 3d).

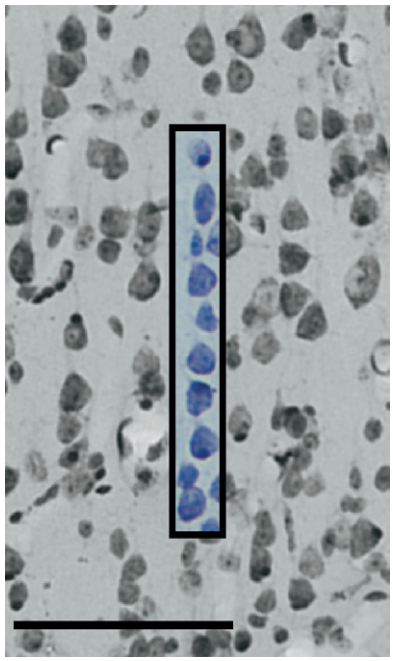

Fig. 2. Photomicrograph illustrating a column of cells (indicated by the box) that are likely part of a microcolumn and are typical of a "columnar" cortex (scale bar=100 μm).

From the resulting density map, we quantify the microcolumnar structure by extracting the following measures (Fig. 3e):

- S, strength of microcolumns (dimensionless ratio of the neuronal density within a microcolumn to the average neuronal density of the ROI),
- T, degree of microcolumnar periodicity (dimensionless ratio of the neuronal density of neighboring microcolumns to the average neuronal density),
- W, microcolumnar width,
- P, distance between microcolumns,
- L, length (vertical span) of microcolumns,
- Y, distance between neurons within a microcolumn (perpendicular to pia and parallel to microcolumns).

In this study, one density map per monkey per area (dorsal or ventral) was calculated using for each area the eight images acquired as described above (see Digital photography section in Experimental Procedures above). From each density map the six microcolumnar properties plus the neuronal density were then calculated. Thus, for each subject two sets of microcolumnar properties were obtained, one for each area (dorsal and ventral).

Behavioral assessment of young adult and aging rhesus monkeys

Monkeys were given a battery of behavioral tests known to be sensitive to age-related cognitive impairments (Herndon et al., 1997). These tests included the Delayed Non-match to Sample test (DNMS), both its acquisition (learning) at a 10 s delay (DNMS-10) and DNMS performance (recognition memory) at longer delays (2 min delay, DNMS-120), and the Delayed Recognition Span Task (DRST) which is a test of working memory span and is given in both

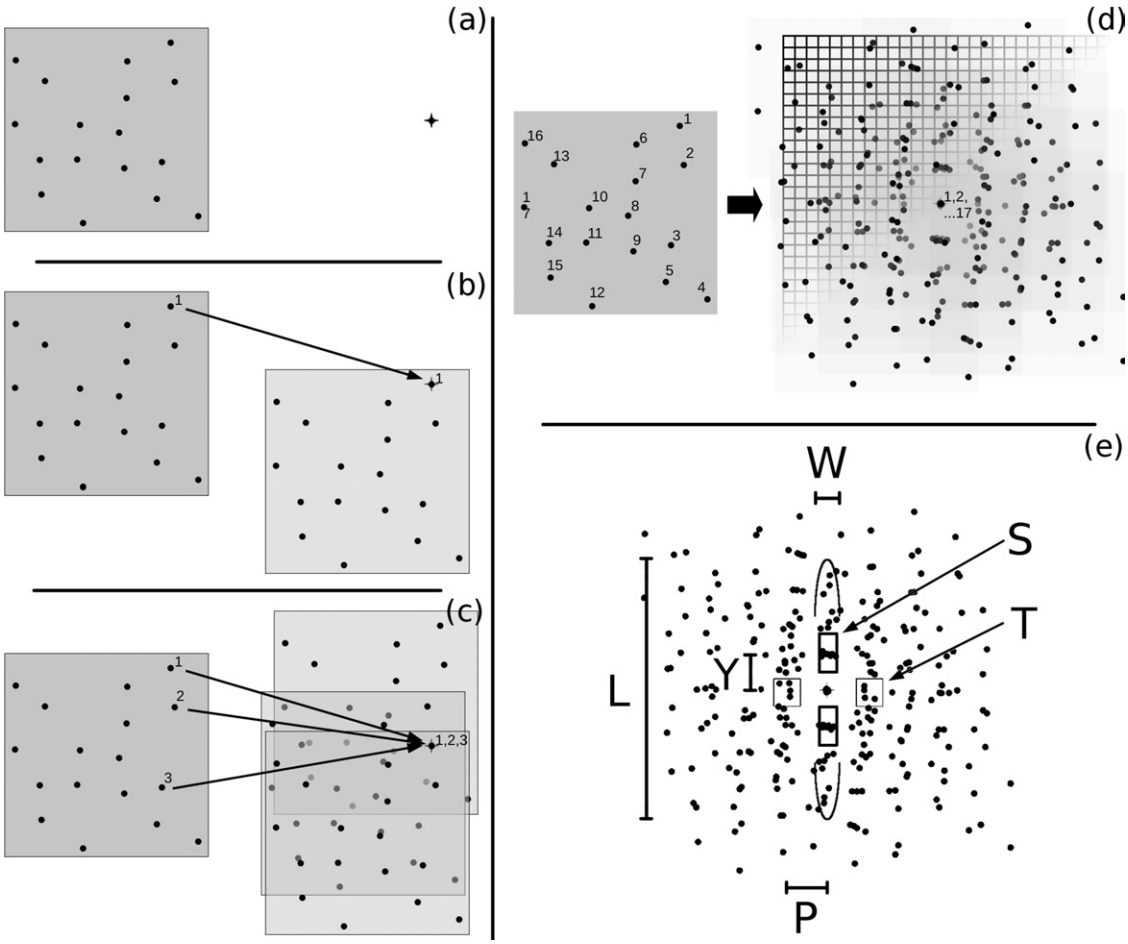

Fig. 3. Schematic diagram illustrating the construction of a density map. (a) Neuronal coordinates (*x,y*) are identified (inside shaded box) and an origin outside the image, marked by a star, is chosen. A copy of the coordinates is made and is shifted so that the neuron identified by the number 1 overlies the origin (b). (c) Three copies corresponding to three different neurons are overlaid on the same origin. This process continues for all of the identified neurons to obtain a single overlay of the positions of all the neurons, shown for this example at the right of the arrow in (d). A grid is then defined in (d) creating a matrix, or density map, whose elements are the number of neurons inside each bin. (e) The definitions of the microcolumnar properties are depicted. The microcolumnar strength *S* and periodicity *T* are calculated as the density of neurons in the indicated boxes divided by the total density of the sample. The width *W* and the length *L* correspond to the width and length of the central microcolumn, as marked in the figure where the semi-ellipsoids indicate the extent of the microcolumn. The distance *P* is the distance between the central microcolumn and nearest microcolumns. The distance *Y* is the distance from the origin (star) to the highest density points inside the box used to calculate *S*. This distance corresponds to the distance between any neuron and its upper or lower neighbor neurons within the same microcolumn.

spatial and object modalities. We also calculated the Cognitive Impairment Index (CII) which is a composite average of the impairment in z-scores relative to young adults of performance on DNMS-10, DNMS-120, and DRST spatial. The details of these are described in Herndon et al. (1997). The tests are administered in the order listed and are all positively rewarded. For a variety of reasons not all monkeys completed all tests. Studies in monkeys and humans suggest that recognition memory aspects of the DNMS and DRST are largely dependent upon the integrity of the medial temporal lobe limbic system (including the entorhinal, perirhinal, and parahippocampal cortices) while other aspects such as rule learning (DNMS acquisition), working memory, and spatial location on the DRST are largely dependent upon the integrity of the lateral prefrontal cortex including area 46 of the sulcus principalis (Petrides, 2005).

Statistical methods

When comparing means between groups of parameters from our density map analysis *t*-tests with a significance level of $P \leq 0.05$ two-tailed were used. Whenever testing for correlations between two sets of parameters the Spearman's rank correlation coefficient was used. While a more traditional Pearson correlation calculation measures linear trends in data, the Spearman correlation coefficient was used to assess how well the relationship between two variables could be related to an arbitrary monotonic function without making any assumptions about the frequency distribution of the variables, i.e. without the assumption that the relationship between the variables is linear or requiring the variables to be measured on interval scales. For the correlation calculations a significance level to $P \leq 0.05$ two-tailed was used.

RESULTS

As described in the Experimental Procedures section, we examined digital images acquired from ROIs from area 46 in the dorsal ($N=19$) and ventral banks ($N=16$) of sulcus principalis. We note that results from 14 of the 16 monkeys examined for ventral area 46 were studied previously, but

Table 1. Age, number of neurons, total area, and neuronal density for each of the female monkey brains analyzed

		Dorsal (N=19)			Ventral (N=16)		
Case	Age	Number of neurons	Area (microns^2)	Density (neurons/μm^2)	Number of neurons	Area (microns^2)	Density (neurons/μm^2)
2	20.4	1274	869,639.06	0.0014650	1272	842,646.74	0.0015095
20	11.8	1168	777,935.94	0.0015014	1076	903,038.94	0.0011915
23	32.3	1108	776,342.97	0.0014272	848	876,961	0.0009670
26	29	1215	769,847.66	0.0015782	1091	813,187.05	0.0013416
41	31.9	1230	760,883.98	0.0016165	1116	880,355.38	0.0012677
65	32.9	1034	772,062.5	0.0013393	963	866,637.05	0.0011112
76	6.4	1061	773,761.33	0.0013712	1414	867,924.48	0.0016292
77	6.4	1039	798,823.44	0.0013007	1080	832,301.1	0.0012976
90	24.9	1845	781,601.56	0.0023605			
96	9	1043	736,386.33	0.0014164	849	868,018.51	0.0009781
97	8.8	983	768,789.06	0.0012786	771	839,924.97	0.0009179
100	24.7	1256	799,665.63	0.0015707	1187	835,582.74	0.0014206
104	28.9	481	367,912.11	0.0013074	951	844,015.43	0.0011268
119	31	1004	780,706.64	0.0012860	1133	866,540.79	0.0013075
125	19.8	1050	766,764.45	0.0013694	686	790,115.63	0.0008682
129	6.7	794	729,950.78	0.0010877	900	800,796.26	0.0011239
130	7.7	1046	775,167.58	0.0013494			
180	29.6	786	769,381.25	0.0010216			
188	6.5	824	723,244.53	0.0011393	701	860,583.14	0.0008146

only results on microcolumnar strength were reported (Cruz et al., 2004).

In Table 1 we list age, total number of neurons found in all ROIs per monkey, tissue area, and neuronal density for all sections from each of the monkeys analyzed. On average, there were 1037 neurons found per region per monkey over an average tissue area of about 796,786 μm^2 per region per monkey.

When analyzing all the cases as one population, we find that the average density is $<\rho>=0.001305\pm0.000282$ neurons/μm^2. When grouping neuronal density by region (dorsal or ventral), the average neuronal density is $<\rho>_D=0.001410\pm0.000064$ neurons/μm^2 in 46D and $<\rho>_V=0.001180\pm0.000059$ neurons/μm^2 in 46V (Table 2). This difference between the densities in the two regions is statistically significant (P=0.012). In Fig. 4a we show the individual neuronal densities ρ (in units of thousandths of neurons per μm^2) as a function of age. This graph shows that there is no significant effect of age on neuronal density confirming previous reports that neurons from area 46 are not lost with age (Peters et al., 1994; Smith et al., 2004).

Table 2. Average values of measures of microcolumnarity

	Dorsal	Ventral
S	1.202	1.207
T	1.06*	0.98*
P	26.52 μm	25.79 μm
W	12.592μm	11.959 μm
L	35.3* μm	40.5* μm
Y	18.1* μm	21.0* μm
ρ	0.00141* neu./μm^2	0.00118* neu./μm^2

* Significantly different, $P<0.05$.

Microcolumnar measures

Microcolumnar parameters. Similar to neuronal density, the measures of microcolumnar organization derived from the density map, with the exception of microcolumnar strength (see below), do not show significant changes with age. In particular, Fig. 4b shows the microcolumnar width W. The population average is $<W>=12.303\pm0.552$ μm with region averages $<W>_D=12.592\pm0.873$ μm and $<W>_V=11.959\pm0.641$ μm which are not significantly different. This figure also shows that there is no significant change of microcolumnar width with age.

The distance between microcolumns P has a population average of $<P>=26.188\pm1.400$ μm. When comparing this by region we found that on average $<P>_D=26.52\pm1.92$ μm and $<P>_V=25.79\pm2.11$ μm, which is not significantly different. Moreover, like W, there is no significant change in the distance between microcolumns with age as shown in Fig. 4c.

Fig. 4d and e shows the degree of microcolumnar periodicity T and length L. Their population averages are $<T>=1.024\pm0.014$ and $<L>=37.66\pm0.93$ μm. The average values of T grouped by region are $<T>_D=1.06\pm0.02$ and $<T>_V=0.98\pm0.02$ and the average values of the length $<L>_D=35.25\pm0.95$ μm and $<L>_V=40.53\pm1.40$ μm where both differences in T and in L per region are significant (P=0.002 for T; P=0.004 for L). However, similar to W and P, no significant age-related changes in either of these parameters with age are detected.

The population average for the vertical distance between neurons within a microcolumn Y (i.e. neuron-neuron distance along the microcolumn) is $<Y>=19.43\pm0.45$ μm. Grouping by region we found that on average, values for Y are $<Y>_D=18.09\pm0.29$ μm and $<Y>_V=21.03\pm0.77$ μm,

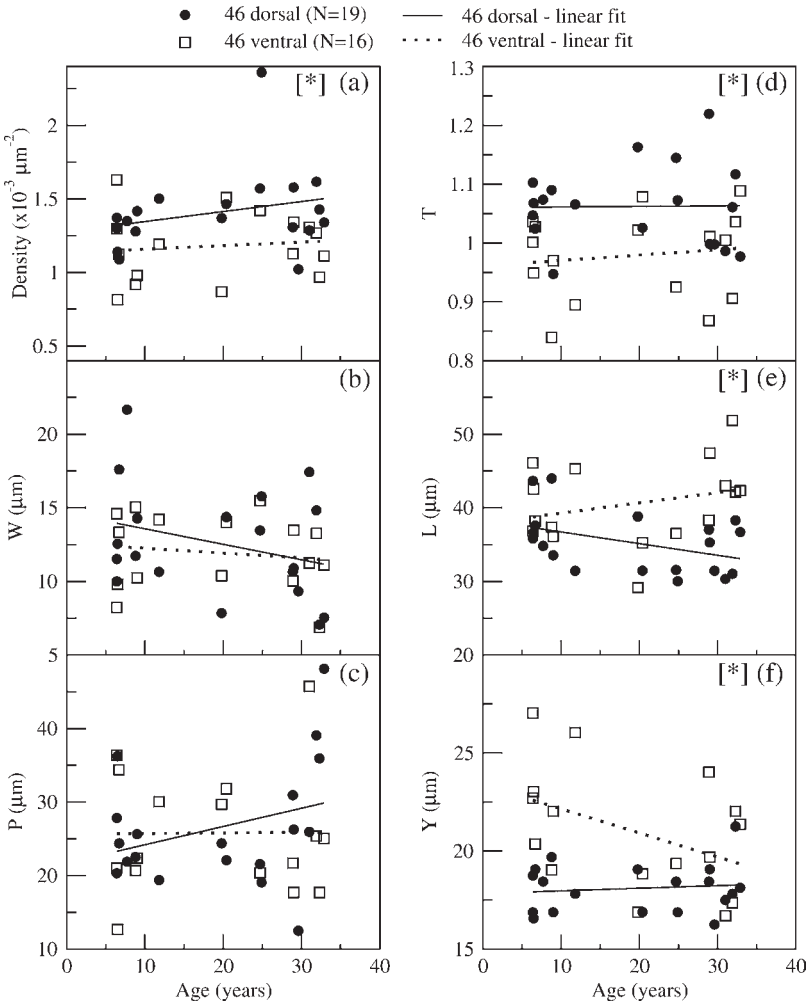

Fig. 4. Neuronal density and microcolumnar properties for all of the cases analyzed. Bullets correspond to dorsal area (N=19) while open squares correspond to the ventral area (N=16). The graphs correspond to (a) neuronal density ρ, (b) width W, (c) inter-column distance P, (d) degree of microcolumnar periodicity T, (e) length L, and (f) interneuronal distance of microcolumns Y. The lines are regression (best fit) lines. Asterisks indicate quantities that are significantly different between groups.

which are significantly different (P=0.002). However, when plotted as a function of age, Y also does not show any significant age-related change (Fig. 4f).

Microcolumnar strength. The average strength of microcolumns S (ratio of the density of neurons in the microcolumn to the total density of neurons in the ROI) for the whole population is $<S>=1.204\pm0.013$. When grouping by region we obtain $<S>_D=1.202\pm0.020$ for 46D and $<S>_V=1.207\pm0.018$ for 46V with no statistically significant difference between the two areas. Fig. 5a and b shows S per region vs. age and documents a significant age-related reduction in S as a function of age in both area 46D and 46V (we plot S-1 instead of S to obtain a quantity that is zero when there is no microcolumnarity). These data confirm our previous findings based on some of the same subjects for 46V (Cruz et al., 2004) and extend the observation of an age-related alteration in microcolumnar strength to the larger cohort in 46V as well as to 46D.

To test whether S_D and S_V correlate with each other we plot in Fig. 5c S_V vs. S_D where each point corresponds to one case and the axes correspond to the microcolumnar strength in the dorsal and ventral region of each case. Analysis of the scatterplot in Fig. 5c shows that there is no significant correlation between S_D and S_V within individuals, suggesting that despite the effect of age on the strength of microcolumns, this effect is not strongly correlated between the two areas within individual subjects.

Relationship to behavior

All of the behavioral tests considered in this paper are sensitive to age-related cognitive impairments (Herndon et al., 1997). In our cohort of monkeys, however, only three behavioral tests show a significant change with age: (i) the CII (Fig. 6a), (ii) a spatial working memory span task, DRST *spatial* (Fig. 6b), and (iii) the acquisition at a 10 s delay of the DNMS test, DNMS-10 (Fig. 6c). The acquisition at a 2 min delay of the DNMS test, DNMS-120 (Fig. 6d) does not show changes with age in our cohort.

In Fig. 6e to l we show all of the cognitive tests versus S_D and S_V. These plots show that there is no significant

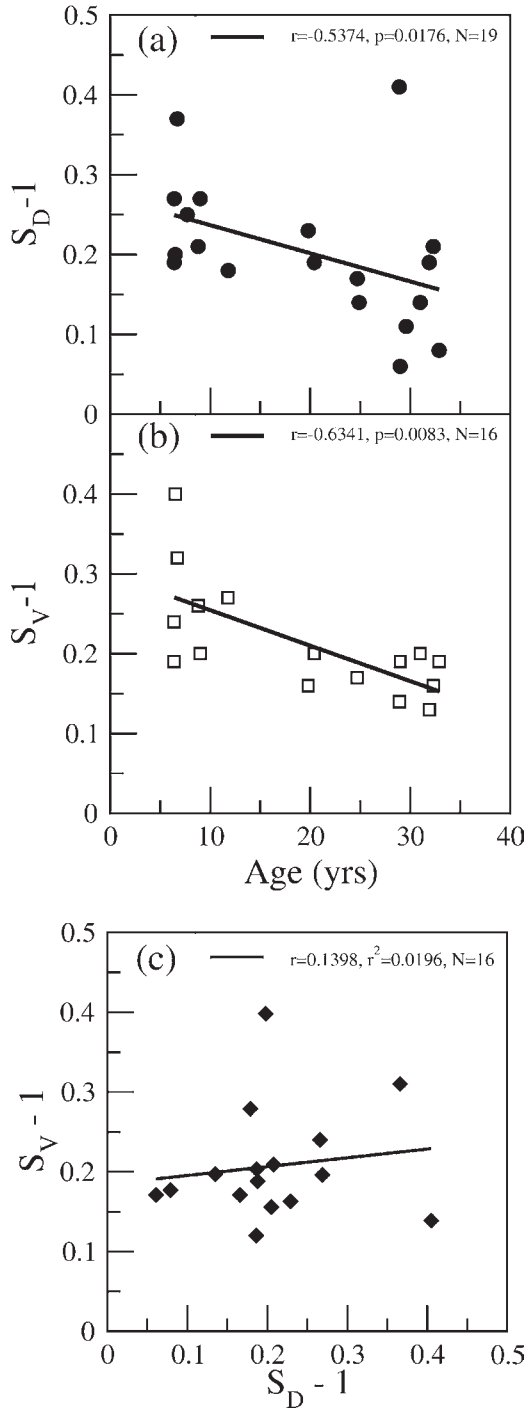

Fig. 5. Microcolumnar strength per case for (a) dorsal S_D ($N=19$) and (b) ventral S_V areas ($N=16$). In both areas the microcolumnar strength decays with age where the correlations are significant. The values of strength are plotted subtracting 1 ($S-1$) to indicate that a zero value of S corresponds by definition to a lack of microcolumnar organization. The lines are regression (best fit) lines. (c) Plot of S_V vs. S_D to determine possible correlations between microcolumnar strength from both areas. The small value for the correlation coefficient indicates a lack of correlations between these two quantities.

relationship between any of the tests and S_D. We also observe that the CII significantly correlates with S_V.

DISCUSSION

Summary

In this paper we use a density map method to quantify the changing structure of microcolumns in two distinct parts of area 46—the dorsal and ventral banks of the middle level of sulcus principalis of the prefrontal cortex—in behaviorally characterized aging female monkeys. This quantitative analysis demonstrates that while many microcolumnar properties are similar between area 46 in the dorsal and ventral banks, there are differences in others. Moreover, while there are age-related effects in both areas, only the changes in ventral area 46 show a relationship with aging.

Basic properties of microcolumns

Our density map method allows us to quantify and explore changes in microcolumnar structure by assessing subtle alterations in the spatial organization of neurons. With this method we find that the microcolumnar strength S does not differ significantly between 46D and 46V. In contrast, we find significant differences between areas 46D and 46V in the global neuronal density ρ, the effective microcolumn length L, the degree of microcolumnar periodicity T, and the interneuronal vertical distance Y within the microcolumns. Specifically, 46D has an overall greater neuronal density and evinces a stronger degree of microcolumnar periodicity than 46V. In contrast, 46V exhibits longer effective microcolumnar lengths L and increased distance between neurons within microcolumns Y. A possible explanation for the coincident larger L and Y values in 46V is that both of these measures depend on the angle of cut of the tissue sections, i.e. perpendicular cuts to the pia may preserve longer columns and record larger Y distances due to the smaller projection angle as opposed to more oblique cuts. Because of intrinsic experimental difficulties in determining the angle of cut of each section, we are currently investigating the correlation between L and Y as a function of angle of cut by means of our three-dimensional computational model (Cruz et al., 2008).

Microcolumnar properties and age

While the microcolumnar strength does not differ between 46D and 46V, there is a significant age-related reduction in S for both areas. This reduction in microcolumnar strength is more than a statistical property of the tissue and can be visualized as a literal loss of microcolumnar organization. In Fig. 7 we show two images from each of three cases studied here for which their values of S span the numerical range observed in this study. The top row consists of two images depicting a case with stronger microcolumnarity (a–b) than the two other cases ((c–d) and (e–f)), indicated by the numerical value of S for each case.

Interestingly, even though S declines with age in both areas, only in 46V does this decline correlate with the CII, a composite measure of the impairment indicated by the DNMS-10, DNMS-120, and DRST *spatial* scores. By comparing S_V with S_D we further show that these two quantities do not correlate with each other, suggesting that although

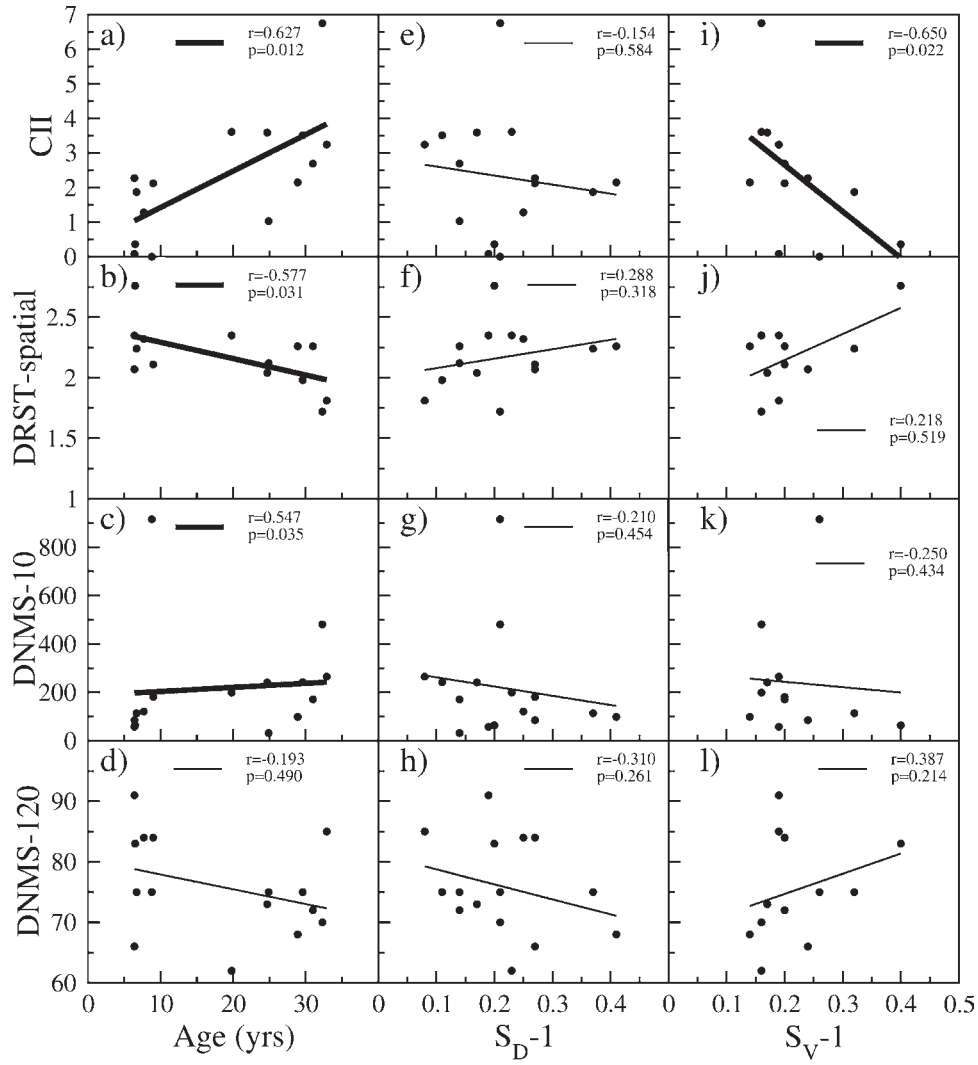

Fig. 6. Plots of cognitive tests vs. age, S_D, and S_V. The tests include a global CII, a spatial working memory span task (DRST-*spatial*), the acquisition at a 10 s delay of the DNMS-10, and recognition memory performance of DNMS-120. Plots showing significant correlations are marked with thick linear fits. For the monkeys from our cohort, only (a) CII, (b) DRST-spatial, and (c) DNMS-10 correlate with age. Correlations between behavior and *S* show that CII correlates with S_V (i).

both decay with age, the two changes are independent and only S_V correlates with the cognitive tests considered in this paper. The fact that the age-related loss of microcolumnar strength in 46D does not correlate with the age-related behavioral impairments in this group of subjects while the loss of strength in 46V does, likely reflects the differential function of these two areas. Petrides (2000b, 2005) reviewed data on both the differential function and connectivity of 46D and 46V and concluded that these two areas had specialized functions. While the exact nature of these functions still remains to be determined, the executive function and temporal ordering that Petrides ascribed to 46D seems unlikely to be directly tapped by the battery of memory tasks available on this cohort of subjects. In contrast, the involvement in memory functions that Petrides ascribed to 46V is supported by the behavioral deficits observed in our cohort of subjects.

Insights into possible mechanisms using a computational approach

The reported age-related change in microcolumnar strength *S* raises the question of possible mechanisms underlying this change. There are numerous neurobiological variables that could be related to this change. To gain some insight into which of these variables are relevant, and thus possible underlying mechanism(s), we previously developed a two-dimensional computational model (Cruz et al., 2004) to explore possible relationships between loss of microcolumnar strength and age-related changes in neuronal locations in the cortex given that the number of neurons and neuronal density do not change with age. Using this model, we demonstrated that the observed reduction of microcolumnar strength in 46V observed in aged monkeys could be accounted for if neuron locations in layer 3 of an average young monkey were computationally displaced by small random increments with an

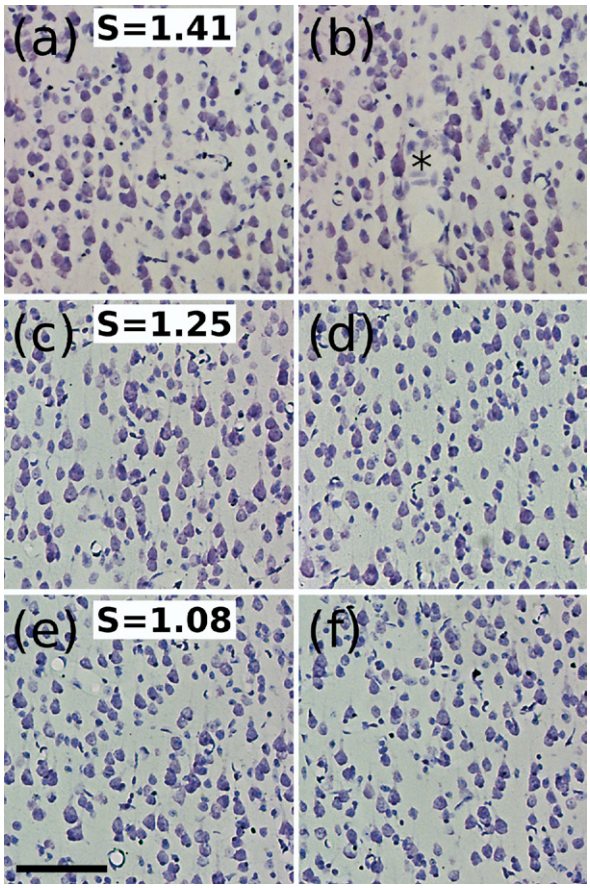

Fig. 7. Illustration of the correspondence between calculated microcolumnar strength *S* and the microcolumnarity (vertically oriented) of tissue sections. The two photomicrographs in each row ((a–b), (c–d), and (e–f)) are typical photomicrographs from each of three cases along with the value of *S* for each case (inset value). We note that *S* was calculated using all eight photomicrographs as described in Digital Photography section. From this illustration one can qualitatively appreciate that as the value of *S* decreases (downward), the visual degree of microcolumnarity also decreases. To ease in the comparison, the images were matched for approximate neuronal density and span the range of obtained values for *S*. For the calculation of microcolumnar properties, regions in the images containing artifacts such as tissue folds or blood vessels (asterisk in b) are computationally excluded by digitally masking the region. The scale bar=100 μm for all panels.

overall average displacement of about 3 μm, i.e. less than a neuronal radius. Close inspection of the neuronal distributions generated using this computational model corroborated that these distributions visually resembled those typically found in tissue, such as those depicted in Fig. 7, when matched to similar values of *S*.

Such small displacements could result from many factors but illustrate the subtle nature of the change that can be detected with the density map method without the need of gross pathology. An ongoing study extending this computational model of small neuronal displacements to three-dimensions (Cruz et al., 2008; Cruz et al., unpublished observations) shows that these conclusions are preserved when the z dimension is considered in the computational model.

Potential biological mechanisms

Based on our findings, it is plausible that the observed changes in microcolumnar measures reflect subtle age-related displacements in neuron location. Although this conclusion by itself does not establish a biological mechanism for such displacements, it suggests a number of possible candidates. It is clear that the brain is dynamic and changing throughout the lifespan. Synapses change morphology on a time scale of minutes to hours in response to long-term potentiation (Leuner et al., 2003; Lynch, 2004; Lambrecht and LeDoux, 2004). Synaptic plasticity is also seen in response to hormonal manipulations, though the time scale for morphological changes is on the order of a month (Weeks, 2003). Dendrites also sprout or regress (Weeks, 2003; Grill and Riddle, 2002). There is growing evidence that even in the adult brain new neurons are generated and integrate themselves into functional circuits (Shors et al., 2001). Furthermore, while it is increasingly difficult to find evidence for significant neuronal loss in normal aging, the literature on aging provides evidence of a variety of changes in layer 3 neurons in the aging brain. Page et al. (2002), Duan et al. (2003), Morrison and Hof (2007) and Dickstein et al. (2007) have all documented dendritic atrophy including changes in branching patterns and spine density. In addition, while basic membrane properties of layer 3 pyramidal neurons are preserved, there are changes in synaptic input and action potential generation that also indicate significant alterations in function (e.g. Luebke et al., 2004; Chang et al., 2005). There are also a variety of degenerative changes in myelin (Peters 2002), and even loss of cortico-cortical axons (Sandell and Peters, 2003), which generally originate from layer 3 where our measurements were conducted. Consequently, it is plausible that one or more of these brain changes contribute to the observed subtle displacements of neurons and may underlie our measured changes in the strength of microcolumnarity.

CONCLUSION

The quantitative density map approach utilized in this study demonstrates age-related changes in measures of microcolumnarity in area 46 of the prefrontal cortex. Our study shows that there is an age-related loss of microcolumnar strength in both 46D and 46V, however, only the loss of microcolumnar strength in 46V is associated with age-related cognitive impairment in a global CII that assesses learning, recognition memory, and working memory. These data are also consistent with the view that a loss in the strength of microcolumns is a consequence of subtle changes in the organization of neurons within microcolumns, but because subtle changes in complex systems can cause significant changes due to their interconnectivity and cooperativity, these changes may have functional consequences for information processing in the aging brain. The data also demonstrate that even within parts of the same cytoarchitectonic area, there may be further subtle anatomical and functional dissociations that are discernible with the methods we have developed. Finally, if the reductions in *S* with age in both areas exam-

ined reflect a more global age-related disruption that results in a loss of neuronal coherence within microcolumns throughout the brain, the lack of correlation with age-related cognitive impairment for the measures of 46D implies that our battery of behavioral tests is insensitive to the functional changes in that area.

Software

The code containing the density map method used in this work to quantify microcolumns is available in the download section of www.physics.drexel.edu/~ccruz/micros/.

Acknowledgments—This work was supported by the National Institutes of Health grants R01-AG021133, P01-AG000001 and P51-RR00165, the Alzheimer Association, and the Bechtel Foundation.

REFERENCES

Benes FM, Bird ED (1987) An analysis of the arrangement of neurons in the cingulate cortex of schizophrenic patients. Arch Gen Psychiatry 44:608–616.

Buldyrev SV, Cruz L, Gomez-Isla T, Gomez-Tortosa E, Havlin S, Le R, Stanley HE, Urbanc B, Hyman BT (2000) Description of microcolumnar ensembles in association cortex and their disruption in Alzheimer and Lewy body dementias. Proc Natl Acad Sci U S A 97:5039–5043.

Buxhoeveden DP, Casanova MF (2002) The minicolumn and evolution of the brain. Brain Behav Evol 60:125–151.

Buxhoeveden D, Casanova MF (2005) Encephalization, minicolumns, and hominid evolution. In: Neocortical modularity and the cell minicolumn (Casanova MF, ed), pp 117–136. New York: Nova Science Publishers.

Buxhoeveden D, Roy E, Switala A, Casanova MF (2000) Reduced interneuronal space in schizophrenia. Biol Psychiatry 47:681–683.

Buxhoeveden D, Fobbs A, Roy E, Casanova M (2002) Quantitative comparison of radial cell columns in children with Down's syndrome and controls. J Intellect Disabil Res 46:76–81.

Buxhoeveden DP, Hasselrot U, Buxhoeveden NE, Booze RM, Mactutus CF (2006) Microanatomy in 21 day rat brains exposed prenatally to cocaine. Int J Dev Neurosci 24:335–341.

Casanova MF, Buxhoeveden DP, Cohen M, Switala AE, Roy EL (2002) Minicolumnar pathology in dyslexia. Ann Neurol 52:108–110.

Casanova MF, Buxhoeveden D, Gomez J (2003) Disruption in the inhibitory architecture of the cell minicolumn: Implications for autism. Neuroscientist 9:496–507.

Chang Y-M, Rosene DL, Killiany RJ, Mangiamele LA, Luebke JI (2005) Increased action potential firing rates of layer 2/3 pyramidal cells in the prefrontal cortex are significantly related to cognitive performance in aged monkeys. Cereb Cortex 15:409–418.

Constantinidis C, Franowicz MN, Goldman-Rakic PS (2001) Coding specificity in cortical microcircuits: a multiple-electrode analysis of primate prefrontal cortex. J Neurosci 21:3646–3655.

Cruz L, Roe DL, Urbanc B, Cabral H, Stanley HE, Rosene DL (2004) Age-related reduction in microcolumnar structure in area 46 of the rhesus monkey correlates with behavioral decline. Proc Natl Acad Sci U S A 101:15846–15851.

Cruz L, Buldyrev SV, Peng S, Roe DL, Urbanc B, Stanley HE, Rosene DL (2005) A statistically based density map method for identification and quantification of regional differences in microcolumnarity in the monkey brain. J Neurol Methods 141:321–332.

Cruz L, Urbanc B, Inglis A, Rosene DL, Stanley HE (2008) Generating a model of the three-dimensional spatial distribution of neurons using density maps. Neuroimage 40:1105–1115.

DeFelipe J, Hendry SHC, Hashikawa T, Molinari M, Jones EG (1990) A microcolumnar structure of monkey cerebral-cortex revealed by immunocytochemical studies of double bouquet cell axons. Neuroscience 37:655–673.

Dickstein DL, Kabaso D, Rocher AB, Luebke JI, Wearne SL, Hof PR (2007) Changes in the structural complexity of the aged brain. Aging Cell 6:275–284.

Duan H, Wearne SL, Rocher AB, Macedo A, Morrison JH, Hof PR (2003) Age-related dendritic and spine changes in corticocortically projecting neurons in macaque monkeys. Cereb Cortex 13:950–961.

Goldman PS, Rosvold HE (1970) Localization of function within the dorsolateral prefrontal cortex of the rhesus monkey. Exp Neurol 27:291–304.

Goldman PS, Rosvold HE, Vest B, Galkin TW (1971) Analysis of the delayed alternation deficit produced by dorsolateral prefrontal lesions in the rhesus monkey. J Comp Physiol Psychol 77:212–220.

Goldman-Rakic PS (1988) Topography of cognition: Parallel distributed networks in primate association cortex. Annu Rev Neurosci 11:137–156.

Grill JD, Riddle DR (2002) Age-related and laminar-specific dendritic changes in the medial frontal cortex of the rat. Brain Res 937:8–21.

Helmstaedter M, de Kock CPJ, Feldmeyer D, Bruno RM, Sakmann B (2007) Reconstruction of an average cortical column in silico. Brain Res Rev 55:193–203.

Herndon JG, Moss MB, Rosene DL, Killiany RJ (1997) Patterns of cognitive decline in aged rhesus monkeys. Behav Brain Res 87:25–34.

Horton JC, Adams DL (2005) The cortical column: a structure without a function. Phil Trans R Soc B 360:837–862.

Hubel DH, Wiesel TN (1963) Shape and arrangement of columns in cat's striate cortex. J Physiol 165:559–568.

Hubel DH, Wiesel TN (1969) Anatomical demonstration of columns in the monkey striate cortex. Nature 221:747–750.

Hubel DH, Wiesel TN (1977) Functional architecture of macaque visual cortex. Proc R Soc Lond B 198:1–59.

Inglis A, Cruz L, Roe DL, Stanley HE, Rosene DL, Urbanc B (2008) Automated retrieval of neuron location from Nissl-stained tissue. J Microsc 230:339–347.

Jones EG (2000) Microcolumns in the cerebral cortex. Proc Natl Acad Sci U S A 97:5019–5021.

Krieger P, Kuner T, Sakmann B (2007) Synaptic connections between layer 5B pyramidal neurons in mouse somatosensory cortex are independent of apical dendrite bundling. J Neurosci 27:11473–11482.

Lambrecht R, LeDoux J (2004) Structural plasticity and memory. Nat Rev Neurosci 5:45–54.

Leuner B, Falduto J, Shors T (2003) Associative memory formation increases the observation of dendritic spines in the hippocampus. J Neurosci 23:659–665.

Leventhal AG, Wang Y, Pu M, Zhou Y, Ma Y (2003) GABA and its agonists improved visual cortical function in senescent monkeys. Science 300:812–815.

Luebke JI, Chang Y-M, Moore TL, Rosene DL (2004) Normal aging results in decreased synaptic excitation and increased synaptic inhibition of layer 2/3 pyramidal cells in the monkey prefrontal cortex. Neuroscience 125:277–288.

Lynch MA (2004) Long-term potentiation and memory. Physiol Rev 84:87–136.

Moore TL, Killiany RJ, Herndon JG, Rosene DL, Moss MB (2002a) Impairment in abstraction and set shifting in aged rhesus monkeys. Neurobiol Aging 5717:1–10.

Moore TL, Killiany RJ, Rosene DL, Prusty S, Hollander W, Moss MB (2002b) Impairment of executive function induced by hypertension in the rhesus monkey (Macaca mulatta). Behav Neurosci 116:387–396.

Moore TL, Killiany RJ, Herndon JG, Rosene DL, Moss MB (2005) A non-human primate test of abstraction and set shifting: An automated adaptation of the Wisconsin Card Sorting Test. J Neurosci Methods 146:165–173.

Morrison JH, Hof PR (2007) Life and death of neurons in the aging cerebral cortex. Int Rev Neurobiol 81:41–57.

Mountcastle VB (1957) Modality and topographic properties of single neurons of cat's somatic sensory cortex. J Neurophysiol 20:408–434.
Mountcastle VB (1997) The columnar organization of the neocortex. Brain 120:701–722.
Mountcastle VB (2003) Introduction [untitled]. Cereb Cortex 13:2–4.
Page TL, Einstein M, Duan H, He Y, Flores T, Rolshud D, Erwin JM, Wearne SL, Morrison JH, Hof PR (2002) Morphological alterations in neurons forming corticocortical projections in the neocortex of aged Patas monkeys. Neurosci Lett 317:37–41.
Pakkenberg B, Gundersen HJG (1997) Neocortical neuron number in humans: Effect of sex and age. J Comp Neurol 384:312–320.
Pakkenberg B, Pelvig D, Marner L, Bundgaard MJ, Gundersen HJG, Nyengaard JR, Regeur L (2003) Aging and the human neocortex. Exp Gerontol 38:95–99.
Peters A (1994) The organization of the primary visual cortex in the macaque. In: Cerebral cortex, Vol. 10 (Peters A, Rockland KS, eds), pp 1–35. New York: Plenum Press.
Peters A (2002) The effects of normal aging on myelin and nerve fibers: A review. J Neurocytol 31:581–593.
Peters A, Rosene DL (2003) In aging, is it gray or white? J Comp Neurol 462:139–143.
Peters A, Sethares C (1996) Myelinated axons and the pyramidal cell modules in monkey primary visual cortex. J Comp Neurol 365:232–255.
Peters A, Leahu D, Moss MB, McNally KJ (1994) The effects of aging on area-46 of the frontal-cortex of the rhesus-monkey. Cereb Cortex 4:621–635.
Peters A, Morrison JH, Rosene DL, Hyman BT (1998) Feature article: are neurons lost from the primate cerebral cortex during normal aging? Cereb Cortex 8:295–300.
Petrides M, Pandya DN (1994) Comparative architectonic analysis of the human and macaque frontal cortex. In: Handbook of neuropsychology, Vol. 9 (Grafman J, Boller F, eds), pp 17–58. Amsterdam: Elsevier.
Petrides M (2000a) Dissociable roles of mid-dorsolateral prefrontal and anterior inferotemporal cortex in visual working memory. J Neurosci 20:7496–7503.
Petrides M (2000b) The role of the mid-dorsolateral prefrontal cortex in working memory. Exp Brain Res 133:44–54.
Petrides M (2005) Lateral prefrontal cortex: architectonic and functional organization. Phil Trans R Soc B 360:781–795.
Purves D, Riddle DR, LaMantia AS (1992) Iterated patterns of brain circuitry (or how the cortex gets its spots). Trends Neurosci 15:362–368.
Rockland KS, Ichinohe N (2004) Some thoughts on cortical minicolumns. Exp Brain Res 158:265–277.
Rosene DL, Roy NJ, Davis BJ (1986) A cryoprotection method that facilitates cutting frozen sections of whole monkey brains for histological and histochemical processing without freezing artifact. J Histochem Cytochem 34:1301–1315.
Roth GS, Mattison JA, Ottinger MA, Chachich ME, Lane MA, Ingram DK (2004) Aging in rhesus monkeys: Relevance to human health interventions. Science 305:1423–1426.
Sandell JH, Peters A (2003) Disrupted myelin and axon loss in the anterior commissure of the aged rhesus monkey. J Comp Neurol 466:14–30.
Schmolesky MT, Wang Y, Pu M, Leventhal AG (2000) Degradation of stimulus selectivity of visual cortical cells in senescent rhesus monkeys. Nat Neurosci 3:384–390.
Shors TJ, Miesegaes G, Beylin A, Zhao M, Rydel T, Gould E (2001) Neuro-genesis in the adult is involved in the formation of trace memories. Nature 410:372–375.
Smith DE, Rapp PR, McKay HM, Roberts JA, Tuszynski MH (2004) Memory impairment in aged primates is associated with focal death of cortical neurons and atrophy of subcortical neurons. J Neurosci 24:4373–4381.
Swindale NV (1990) Is the cerebral cortex modular? Trends Neurosci 13:487–492.
Tigges J, Gordon TP, McClure JM, Hall EC, Peters A (1988) Survival rate and life span of rhesus monkeys at the Yerkes Regional Primate Research Center. Am J Primatol 15:263–273.
Van Hoesen GW, Solodkin A (1993) Some modular features of temporal cortex in humans as revealed by pathological changes in Alzheimer's disease. Cereb Cortex 3:465–475.
Vercelli AE, Garbossa D, Curtetti R, Innocenti GM (2004) Somatodendritic minicolumns of output neurons in the rat visual cortex. Eur J Neurosci 20:495–502.
Weeks JC (2003) Thinking globally, acting locally: steroid hormone regulation of the dendritic architecture, synaptic connectivity and death of an individual neuron. Prog Neurobiol 70:421–442.

(Accepted 18 November 2008)
(Available online 27 November 2008)